A Physics-Based Compact Model for CIGS and CdTe Solar Cells: From Voltage-Dependent Carrier Collection to Light-Enhanced Reverse Breakdown

Preprint

Xingshu Sun and Muhammad Ashraful Alam
Purdue University

John Raguse
Colorado State University

Rebekah Garris, Chris Deline, and Timothy Silverman
National Renewable Energy Laboratory

Presented at the 42nd IEEE Photovoltaic Specialists Conference
New Orleans, Louisiana
June 14–19, 2015

© 2015 IEEE. Personal use of this material is permitted. Permission from IEEE must be obtained for all other uses, in any current or future media, including reprinting/republishing this material for advertising or promotional purposes, creating new collective works, for resale or redistribution to servers or lists, or reuse of any copyrighted component of this work in other works.

NREL is a national laboratory of the U.S. Department of Energy
Office of Energy Efficiency & Renewable Energy
Operated by the Alliance for Sustainable Energy, LLC

This report is available at no cost from the National Renewable Energy Laboratory (NREL) at www.nrel.gov/publications.

Conference Paper
NREL/CP-5J00-65164
October 2015

Contract No. DE-AC36-08GO28308

NOTICE

The submitted manuscript has been offered by an employee of the Alliance for Sustainable Energy, LLC (Alliance), a contractor of the US Government under Contract No. DE-AC36-08GO28308. Accordingly, the US Government and Alliance retain a nonexclusive royalty-free license to publish or reproduce the published form of this contribution, or allow others to do so, for US Government purposes.

This report was prepared as an account of work sponsored by an agency of the United States government. Neither the United States government nor any agency thereof, nor any of their employees, makes any warranty, express or implied, or assumes any legal liability or responsibility for the accuracy, completeness, or usefulness of any information, apparatus, product, or process disclosed, or represents that its use would not infringe privately owned rights. Reference herein to any specific commercial product, process, or service by trade name, trademark, manufacturer, or otherwise does not necessarily constitute or imply its endorsement, recommendation, or favoring by the United States government or any agency thereof. The views and opinions of authors expressed herein do not necessarily state or reflect those of the United States government or any agency thereof.

This report is available at no cost from the National Renewable Energy Laboratory (NREL) at www.nrel.gov/publications.

Available electronically at SciTech Connect http:/www.osti.gov/scitech

Available for a processing fee to U.S. Department of Energy and its contractors, in paper, from:

U.S. Department of Energy
Office of Scientific and Technical Information
P.O. Box 62
Oak Ridge, TN 37831-0062
OSTI http://www.osti.gov
Phone: 865.576.8401
Fax: 865.576.5728
Email: reports@osti.gov

Available for sale to the public, in paper, from:

U.S. Department of Commerce
National Technical Information Service
5301 Shawnee Road
Alexandra, VA 22312
NTIS http://www.ntis.gov
Phone: 800.553.6847 or 703.605.6000
Fax: 703.605.6900
Email: orders@ntis.gov

Cover Photos by Dennis Schroeder: (left to right) NREL 26173, NREL 18302, NREL 19758, NREL 29642, NREL 19795.

NREL prints on paper that contains recycled content.

Abstract

In this paper, we develop a physics-based compact model for copper indium gallium diselenide (CIGS) and cadmium telluride (CdTe) heterojunction solar cells that attributes the failure of superposition to voltage-dependent carrier collection in the absorber layer, and interprets light-enhanced reverse breakdown as a consequence of tunneling-assisted Poole-Frenkel conduction. The temperature dependence of the model is validated against both simulation and experimental data for the entire range of bias conditions. The model can be used to characterize device parameters, optimize new designs, and most importantly, predict performance and reliability of solar panels including the effects of self-heating and reverse breakdown due to partial-shading degradation.

Index Terms

Analytical model, panel simulation, light-enhanced breakdown, partial shading, voltage-dependent photocurrent

This report is available at no cost from the National Renewable Energy Laboratory (NREL) at www.nrel.gov/publications.

Acronyms and Abbreviations

a-Si	amorphous silicon
CdTe	cadmium telluride
CIGS	copper indium gallium diselenide
cm	centimeter
eV	electron volt
IV	current-voltage
I-V-T	temperature-dependent current-voltage
J	joule
K	kelvin
mA	milliampere
µm	micrometer
mS	milliSiemens
nm	nanometer
NREL	National Renewable Energy Laboratory
PV	photovoltaic
SCAPS	solar cell capacitance simulator
SCL	space-charge-limited
Si	silicon
SPICE	simulation program with integrated circuit emphasis
TCO	transparent conductive oxide
TFPV	thin film photovoltaic technology
V	voltage

This report is available at no cost from the National Renewable Energy Laboratory (NREL) at www.nrel.gov/publications.

Contents

1 Introduction 1
2 Model Development and Validation 2
2.1 Forward Bias IV Characteristics of a Heterojunction Cell 2
2.2 Reverse Breakdown 4
3 Electro-Thermal Panel Simulation 8
4 Conclusion 9
References 10

This report is available at no cost from the National Renewable Energy Laboratory (NREL) at www.nrel.gov/publications.

Figures

Figure 1. The five-parameter model (shifted the dark measurement by a constant short circuit current) cannot describe typical CdTe data 1

Figure 2. The energy diagram of CIGS and CdTe solar cells. The IV characteristics of the cell are dictated by the boundary conditions for electrons and holes. 3

Figure 3. The proposed compact model benchmarked against the results from SCAPS simulation at 250 K, 300 K, and 350 K. The solid line is the SCAPS simulation, and the red triangle is the prediction from the compact model. The temperature increases from right to left. The baseline cell parameters are taken from [26]. 3

Figure 4. Measured temperature-dependent dark and light CdTe IV vs. the results from the compact model. The solid line is the experimental data, and the open circles are the results from the compact model. Also shown are CdTe data (efficiency ~10%) for T = 298 K, 308 K, 318 K. The temperature of each subplot increases from right to left. 4

Figure 5. CIGS measurement vs. the compact model. The solid line is the experimental data, and the open circle is the compact model. CIGS[1] (green) data (efficiency ~17%) is provided by National Renewable Energy Laboratory (NREL) at T = 257 K, 273 K, 293 K; CIGS[2] (red) data (efficiency ~15%) is obtained from Uppsala University [13] from 280 K to 340 K with a 20 K interval. The low short circuit current in CIGS[2] is due to monochromatic light source. The temperature of each plot increases from right to left. 4

Figure 6. Reverse breakdown current via tunneling-assisted Poole-Frenkel mechanism. (a) In darkness, electrons in the valence band in the absorber tunnel to the defect level (red) in the buffer layer then are emitted to the conduction and collected by the electrode. (b) The empty defect state (blue) under illumination allows Poole-Frenkel conduction directly occurring in the absorber. . 5

Figure 7. Benchmark results of temperature-dependent CIGS reverse breakdown IV (solid line) against the compact model (blue square). Data was measured at Uppsala University [13], and temperature varies from 260 K to 340 K with a 20 K interval. (a) Reverse breakdown fitting results in darkness. (b) Reverse breakdown fitting results under illumination. 6

Figure 8. (a) The simulated mini module dimension is 10 cm × 10 cm with 10 scribed cells (10 cm × 1 cm) connected in series. The fifth cell is fully shaded in half; the shading area (black rectangle) is 5 cm × 1 cm. (b) A single cell in the module can be further divided into sub-cells. To properly model the lateral and horizontal current flow, the top and bottom contacts of the sub-cells are connected by the transparent conductive oxide (TCO) ($\boldsymbol{Rsheet = 10\ \Omega/sq}$) and back-contact ($\boldsymbol{Rsheet = 1\ \Omega/sq}$) resistors, respectively. (c) The equivalent circuit of a single sub-cell includes the aforementioned compact model. The parameters and equations of the compact model are summarized in Table 1 and Table 2. A non-linear shunt resistor is also included accounting for the space-charge-limited current, see [33]. 8

Figure 9. (a) The spatial distribution and opacity of the shadow. Regions 1 and 2 are the shaded and unshaded areas of the fifth shaded cell, respectively. Region 3 represents the unshaded cells. (b) The voltage distribution of the module. (c) The current distribution of the module. (d) The temperature profile of the module. 9

Tables

Table 1. Equation List of the Compact Model 7

Table 2. Parameter Summary of the Compact Model 7

This report is available at no cost from the National Renewable Energy Laboratory (NREL) at www.nrel.gov/publications.

1 Introduction

It is well known that partial shading of thin film solar panels can subject the shaded cells into severe reverse breakdown, leading to localized self-heating, and in extreme cases, permanent damage [1]–[4]. In order to simulate these effects at the panel level, the cell-scale compact model must describe the temperature-dependent forward current-voltage (I-V-T) and reverse breakdown characteristics accurately.

Unlike crystalline silicon solar cells, the "superposition principle" (with voltage-independent photocurrent) does not hold for CIGS/CdTe solar cells [5]–[7]. As a result, the classical five-parameter model [8] often fails to describe I-V-T characteristics of these heterojunction cells correctly (see Figure 1). Indeed, Ref. [9] demonstrated significant discrepancy between the model predication using the five-parameter model and the actual panel measurement. In part, the failure of superposition can be attributed to bias-dependent photocurrent. Such models have been developed for p-i-n amorphous silicon solar cells [10]; however, the presence of heterojunction and voltage-dependent depletion region (charge collection region) make it challenging to develop similar models for CIGS and CdTe cells [11], [12].

The compact model to be developed in this paper can model the bias-dependent photocurrent *analytically*, explicitly accounting for the non-uniform photogeneration, conduction band offset, and bias-dependent depletion. In addition, recent studies [13], [14] have reported light-enhanced reverse breakdown in CIGS, namely, the breakdown voltage is reduced under illumination. In our model, the breakdown characteristics are interpreted by tunneling-assisted Poole-Frenkel conduction, which can describe the illumination, thickness, and temperature dependencies observed experimentally. We emphasize that the five-parameter model cannot describe any of these critical features of practical heterojunction cells. The compact model can be inserted into an electro-thermal coupled panel simulation network [15]–[17] to simulate the magnitude and spatial distribution of reverse breakdown and local heating as well as the panel efficiency degradation under different shading conditions.

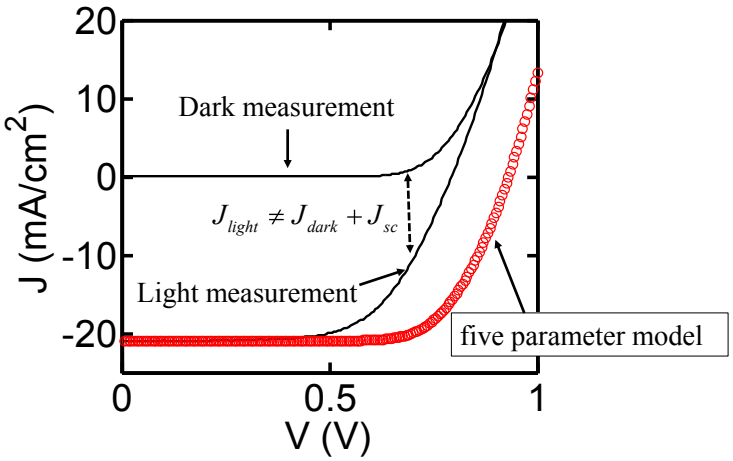

Figure 1. The five-parameter model (shifted the dark measurement by a constant short circuit current) cannot describe typical CdTe data

This report is available at no cost from the National Renewable Energy Laboratory (NREL) at www.nrel.gov/publications.

The paper is organized as follows. The compact model is validated in Section 2 against numerical simulation results as well as experimental measurements, as a function of voltage and temperature. In Section 3, the compact model forms the basis of a panel simulator that can predict the electro-thermal response of a panel under a variety of operating conditions. For an illustrative example, the simulator is used to investigate partial shading of a panel. Section 4 summarizes the conclusions of the paper.

2 Model Development and Validation

2.1 Forward Bias IV Characteristics of a Heterojunction Cell

A typical CIGS (or CdTe) solar cell consists of an ultrathin (~50 nm), but large bandgap buffer layer, stacked on top of a thick absorber layer (~2–3 μm). The energy band diagram of a typical cell is shown in Figure 2.

To obtain the analytical formula of the forward IV characteristics, one must solve the position-resolved electron and hole continuity equations

$$D\frac{\partial^2 n(x)}{\partial x^2} + \mu E(x)\frac{\partial n(x)}{\partial x} + G(x) = 0, \qquad (1)$$

$$D\frac{\partial^2 p(x)}{\partial x^2} - \mu E(x)\frac{\partial p(x)}{\partial x} + G(x) = 0, \qquad (2)$$

with the correct boundary conditions labelled in Figure 2 [18]. The missing bulk recombination term $R(x)$ is effectively accounted in the back surface recombination velocity $s_{n,b}$ as discussed below. Note that at the front contact, the valence band offset at the interface is presumed sufficiently large so that holes cannot exit through the wrong contact, i.e., the hole current to the left contact is zero. At the right edge of the depletion region, the hole concentration is defined by the acceptor doping density, N_A. Similarly, electron transport is defined by two boundary conditions: At the left contact, electrons can be emitted thermionically into the buffer layer, with the emission velocity $s_{n,f} = \frac{v_{th}}{2} e^{-\Delta E_C/kT}$, where the thermal velocity is defined as $v_{th} = \sqrt{\frac{2kT}{\pi m}}$ [19]. A large conduction band offset ΔE_C prevents electrons from being fully collected in the front contact, which in turn distorts the IV characteristics resulting in S shape IV curve [20], [21]. For the right boundary condition for the electrons, we note that the electron current can be defined as $J_n = q s_{n,b} \Delta n$, where Δn is the excess carrier concentration and $s_{n,b}$ represents the effective surface recombination velocity, combining the diffusion velocity in the charge-neutral region and bulk recombination occurring in the depletion region. Any increase in ΔE_C is reflected in Δn, that is, the failure to collect electrons at the left contact is reflected in enhanced recombination in the bulk region.

This report is available at no cost from the National Renewable Energy Laboratory (NREL) at www.nrel.gov/publications.

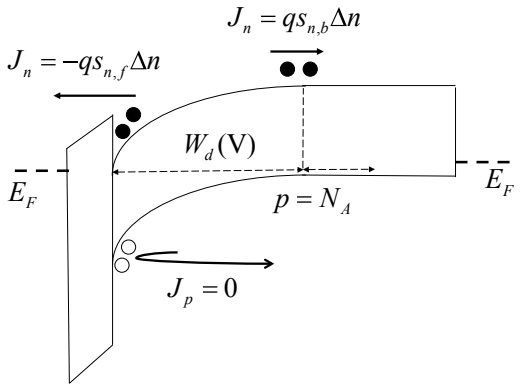

Figure 2. The energy diagram of CIGS and CdTe solar cells. The IV characteristics of the cell are dictated by the boundary conditions for electrons and holes.

Assuming that the optical generation profile decays exponentially into the absorber and that the electric field drops linearly within the depletion region (classical abrupt depletion approximation), one can solve Eqs. 1 and 2 to find the expression for voltage-dependent photocurrent, given by Eq. A in Table 1. The definition of each parameter is listed in Table 2. Equation A will be derived in full in a future publication.

The dark current can be solved analytically as well. For simplicity, however, we assume that the dark current can be represented by a single diode model given by Eq. B in Table 1, characterized by the diode saturation current J_0 and ideality factor n [22]. For now, we ignore the back contact Schottky barrier sometimes observed in CdTe [23], since we have not observed any roll-over effects in the voltage range of interest. This is not a limitation of the model: the Schottky back contact can be accounted by a back-to-back diode circuit [24].

The model validation proceeds in two steps: *first*, we calibrate the model parameters (see Table 2) of the compact model by fitting the room-temperature SCAPS simulation of the same cell [25]. *Second*, we use the temperature dependences of the built-in potential, etc., to extrapolate the room-temperature parameters to other temperatures of interest. Remarkably, the compact model reproduces the temperature dependencies of both the simulated and measured data. The benchmark results against the simulation and experimental data are shown in Figure 3, Figure 4, and Figure 5.

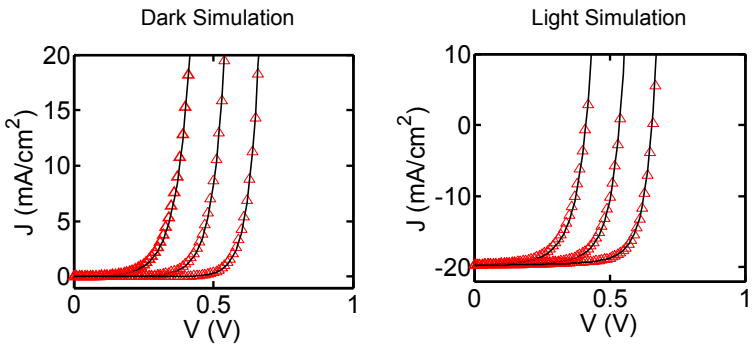

Figure 3. The proposed compact model benchmarked against the results from SCAPS simulation at 250 K, 300 K, and 350 K. The solid line is the SCAPS simulation, and the red triangle is the prediction from the compact model. The temperature increases from right to left. The baseline cell parameters are taken from [26].

This report is available at no cost from the National Renewable Energy Laboratory (NREL) at www.nrel.gov/publications.

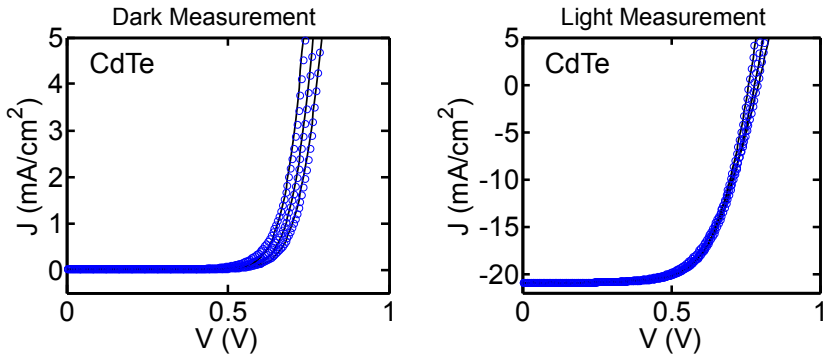

Figure 4. Measured temperature-dependent dark and light CdTe IV vs. the results from the compact model. The solid line is the experimental data, and the open circles are the results from the compact model. Also shown are CdTe data (efficiency ~10%) for T = 298 K, 308 K, 318 K. The temperature of each subplot increases from right to left.

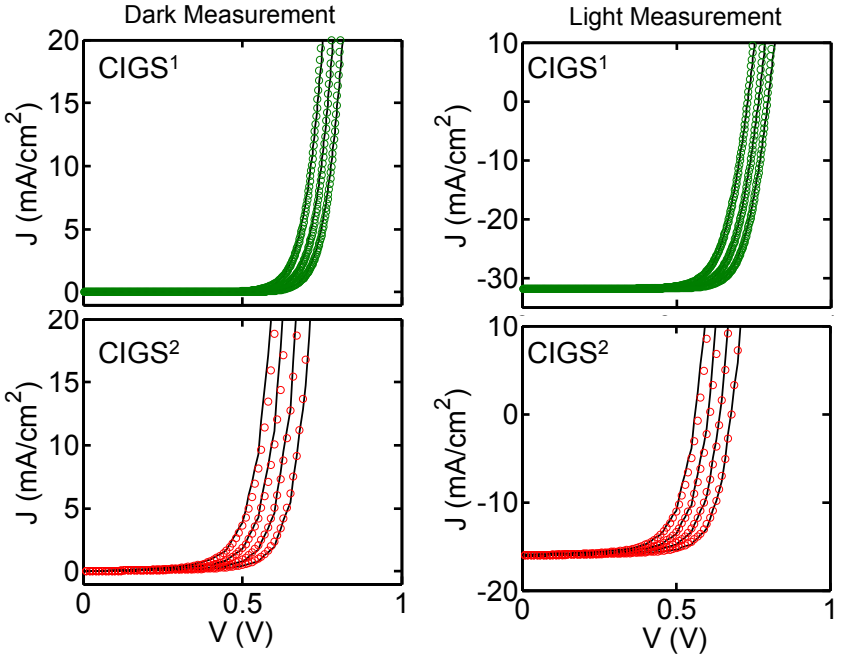

Figure 5. CIGS measurement vs. the compact model. The solid line is the experimental data, and the open circle is the compact model. CIGS[1] (green) data (efficiency ~17%) is provided by National Renewable Energy Laboratory (NREL) at T = 257 K, 273 K, 293 K; CIGS[2] (red) data (efficiency ~15%) is obtained from Uppsala University [13] from 280 K to 340 K with a 20 K interval. The low short circuit current in CIGS[2] is due to monochromatic light source. The temperature of each plot increases from right to left.

2.2 Reverse Breakdown

Partially shaded solar cells in a module can be stressed into reverse breakdown [1]–[4], which results in significant self-heating. Consequently, it is important to include the temperature-dependent breakdown characteristics in the compact model. Interestingly, recent experiments [13], [14] show that the breakdown voltage reduces from -6 V in dark to -2 V under light. Among the various mechanisms, we can exclude avalanche breakdown for the following reasons: Given the doping density of 10^{14} to 10^{17} cm^{-3} [27], the avalanche breakdown voltage is

This report is available at no cost from the National Renewable Energy Laboratory (NREL) at www.nrel.gov/publications.

expected to be from -10 V to -100 V, which is beyond the magnitudes of both the dark and illuminated breakdown voltages observed in the experimental data. Also, as shown in Figure 7, the dark and light breakdown voltages decrease with increasing temperature (i.e., are characterized by a negative temperature coefficient), inconsistent with avalanche breakdown [27], [28].

Similarly, the reverse breakdown cannot be explained by band-to-band tunneling. In general, band-to-band tunneling is indeed described by a negative temperature coefficient because the bandgap shrinks with increasing temperature. The short-circuit current in Figure 4 and Figure 5, however, is independent of temperature, indicating that the bandgap of neither the buffer nor the absorber layer are temperature dependent. Hence, it is unlikely that the reported light-enhanced breakdown is due to band-to-band tunneling, either.

Therefore, we propose to model the reverse breakdown using tunneling-assisted Poole-Frenkel conduction [29], characterized by low breakdown voltage and negative temperature coefficient (see Eq. C in Table 1). As shown in Figure 6, the process of Poole-Frenkel conduction involves the following steps: (1) electrons tunnel toward a defect level elastically; (2) the high electric field lowers the barrier and the temperature assists electrons to emit into the conduction band; and finally, (3) electrons are collected by the contact.

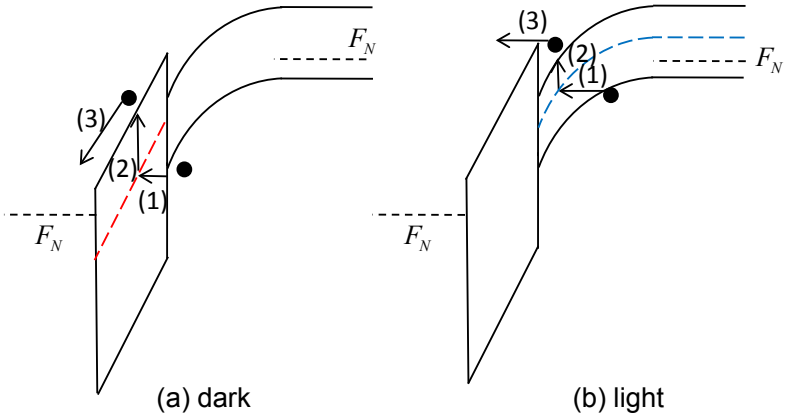

Figure 6. Reverse breakdown current via tunneling-assisted Poole-Frenkel mechanism. (a) In darkness, electrons in the valence band in the absorber tunnel to the defect level (red) in the buffer layer then are emitted to the conduction and collected by the electrode. (b) The empty defect state (blue) under illumination allows Poole-Frenkel conduction directly occurring in the absorber.

This report is available at no cost from the National Renewable Energy Laboratory (NREL) at www.nrel.gov/publications.

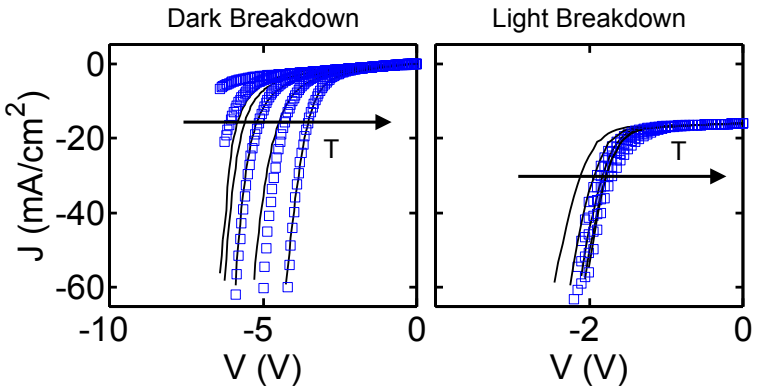

Figure 7. Benchmark results of temperature-dependent CIGS reverse breakdown IV (solid line) against the compact model (blue square). Data was measured at Uppsala University [13], and temperature varies from 260 K to 340 K with a 20 K interval. (a) Reverse breakdown fitting results in darkness. (b) Reverse breakdown fitting results under illumination.

After fitting the Pool-Frenkel model to the experimental data, we find that the model is capable of describing the breakdown characteristics as a function of temperature and voltage under different illumination conditions (see Figure 7). The Poole-Frenkel parameter ($J_{RB0}\sim e^{-E_T/kT}$) depends on the defect level, E_T. The extracted defect level under dark is $E_T \equiv E_C - E_T = 1.2$ eV, whereas the dominant defect level under illumination is 0.36 eV. Hence, we presume that under dark, valence-band electrons from the absorber layer tunnel into a defect level in the buffer layer then emit into the conduction band and finally are collected by the electrode, see Figure 6(a). The reduction in dominant defect level under light could be related to the light-induced metastabilities caused by the V_{Se}-V_{Cu} vacancy complex [30] in the absorber. A much shallower defect-level leads to a larger pre-factor $J_{RB0}\sim e^{-\mathrm{E}_T/kT}$, which explains the reduced breakdown voltage under illumination.

The hypothesis of Poole-Frenkel conduction to model light-enhanced breakdown must be validated by additional experiments. The transition of the breakdown characteristics under different illumination intensity is also not fully understood. To our best knowledge, however, it is the first model that provides an intuitive and quantitative interpretation of the light-enhanced breakdown, and is adequate for the panel-level simulation to be discussed in Section 3.

This report is available at no cost from the National Renewable Energy Laboratory (NREL) at www.nrel.gov/publications.

Table 1. Equation List of the Compact Model

$J_{photo} = J_{tot}\frac{(1-\exp(-\Delta\sqrt{\frac{V_{bi}-V}{V_{bi}}}))}{1+\alpha_C\exp(\beta\frac{(V-V_{bi})}{V_{bi}})}$	(A)
$J_{diode} = J_0(\exp\left(\frac{qV}{nkT}\right)-1)$	(B)
$J_{RB} = J_{RB0}Vexp(\frac{q}{kT}\sqrt{\frac{V}{m}})$	(C)
$J_{shunt} = G_{SH}V + I_{0SH}V^{n_{sh}}$	(D)

Table 2. Parameter Summary of the Compact Model

Parameters	Definition
J_{tot}	total generation current (mA/cm^2)
Δ	product of equilibrium depletion width and average absorption coefficient over the solar spectrum
V_{bi}	junction built-in voltage (V)
β	voltage partition factor
α_C	fitting parameter (ratio between front and back surface recombination velocities)
J_{RB0}	breakdown current prefactor (mA/[Vcm^2])
m	breakdown current index (V$^{-0.5}$)
J_0	diode saturation current (mA/cm^2)
n	diode ideality factor
G_{SH}	ohmic shunt conduction (mS/cm^2)
I_{0SH}	SCL shunt conduction (mS/cm^2)
n_{sh}	SCL shunt index

This report is available at no cost from the National Renewable Energy Laboratory (NREL) at www.nrel.gov/publications.

3 Electro-Thermal Panel Simulation

Partial shading has been recognized as one of the reliability concerns for series-connected solar cell technology, especially in thin film photovoltaic (TFPV) technology. Unlike for crystalline PV technology, monolithic intergradation for creating series connection in TFPV modules makes integration of bypass diode [31] and/or rewiring schemes [32] challenging. One of the consequences of partial shading is reverse stress, since the shaded cells are forced into reverse bias to maintain current continuity with the illuminated cells connected in series. As a result, instead of producing power for the output load, the stressed cells dissipate power to self-heating. For an experimental demonstration of significant self-heating under partial shading, see [2].

To further investigate the degree and spatial distribution of the self-heating effects in a shaded module, we have developed a coupled electro-thermal SPICE model [15]–[17] to describe the operation of the panel (see Figure 8). The subcells in Figure 8(b) are described by the CIGS compact model developed in Section 2, and summarized in Figure 8(c). The subcells are both thermally and electrically connected to their neighbors, as in Figure 8(b). The detailed network setup for the panel simulation will be discussed in the future publication. Note that the simulation is electro-thermally self-consistent because the compact model can accurately describe the temperature dependencies of the forward and reverse IV characteristics.

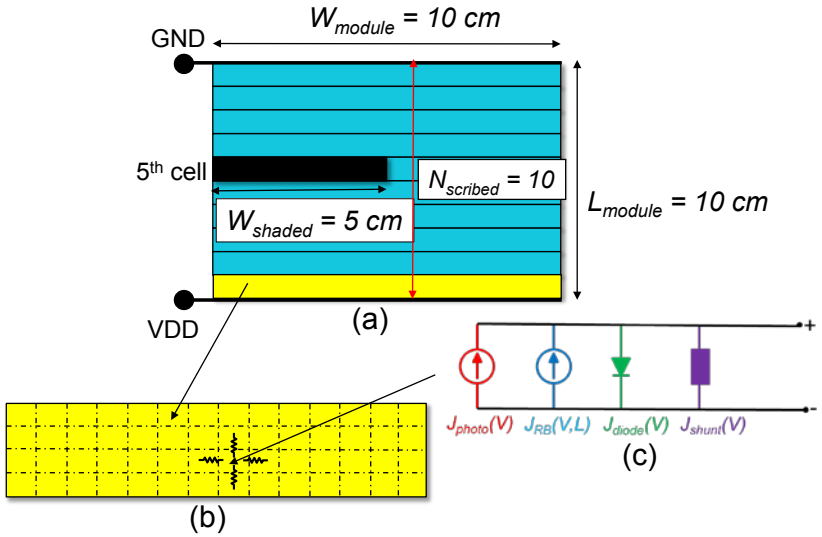

Figure 8. (a) The simulated mini module dimension is 10 cm × 10 cm with 10 scribed cells (10 cm × 1 cm) connected in series. The fifth cell is fully shaded in half; the shading area (black rectangle) is 5 cm × 1 cm. (b) A single cell in the module can be further divided into sub-cells. To properly model the lateral and horizontal current flow, the top and bottom contacts of the sub-cells are connected by the TCO ($R_{sheet} = 10\ \Omega/sq$) and back-contact ($R_{sheet} = 1\ \Omega/sq$) resistors, respectively. (c) The equivalent circuit of a single sub-cell includes the aforementioned compact model. The parameters and equations of the compact model are summarized in Table 1 and Table 2. A non-linear shunt resistor is also included accounting for the space-charge-limited current, see [33].

This report is available at no cost from the National Renewable Energy Laboratory (NREL) at www.nrel.gov/publications.

Figure 9 shows the simulation response of a partially shaded module, biased at the maximum power point associated with the unshaded module. For this illustrative example, we assume that the left half of fifth cell (region 1) is fully shaded, as in Figure 9(a). Since region 1 can no longer produce photocurrent, the need for current continuity with fully illuminated cells in region 3 requires that the shaded cells in regions 1 and 2 be forced into reverse breakdown, as shown in Figure 9(b). Indeed, as shown in Figure 9(c), the current density is extremely high near the edge between the shaded and unshaded areas. The reverse voltage at the boundary is high (around -3 V) resulting in large breakdown current at the illuminated side due to light-enhanced breakdown. The reverse voltage decreases toward right in region 2, therefore, the breakdown current reduces away from the interface between regions 1 and 2 as well. Due to light-enhanced breakdown, the current in the unshaded area (region 2) is much higher than that of the shaded area (region 1); so is the generated heat. Counterintuitively, the temperature rise is more pronounced in the unshaded half of the shaded cell, even though the shaded side operates at higher reverse voltage. The spatial redistribution of the temperature due to partial shading in Figure 9(d) is also in agreement with Figure 5 in [2] and more detailed finite element-based simulation in Ref. [17].

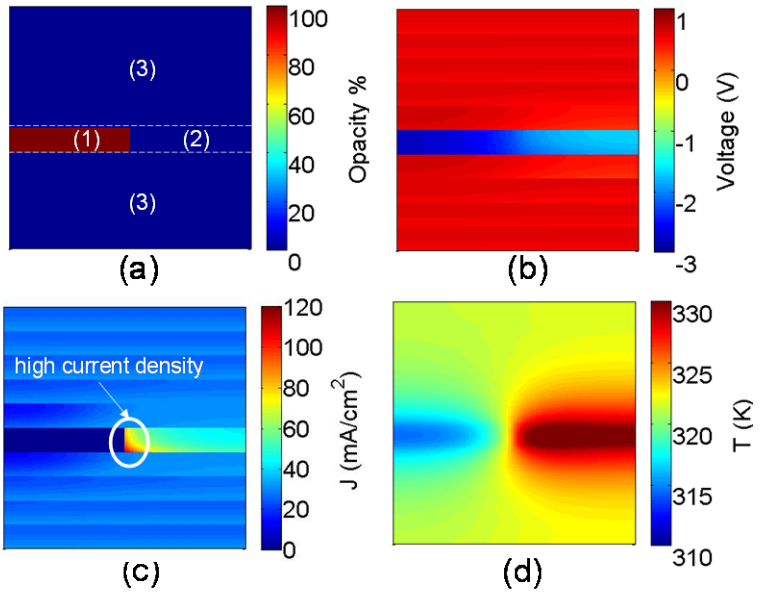

Figure 9. (a) The spatial distribution and opacity of the shadow. Regions 1 and 2 are the shaded and unshaded areas of the fifth shaded cell, respectively. Region 3 represents the unshaded cells. (b) The voltage distribution of the module. (c) The current distribution of the module. (d) The temperature profile of the module.

4 Conclusion

In this paper, we have developed a new physics-based compact model for CIGS and CdTe solar cells and validated the model by comparing against SCAPS-based numerical simulation and experimental data from test samples. In the model, an analytical formulation of the voltage-dependent carrier collection in forward bias explains the failure of superposition, while a tunneling-assisted Poole-Frenkel model interprets light-enhanced reverse breakdown. Once calibrated against the experimental data, the model parameters interpret the salient features of the cell. We developed a self-consistent electro-thermal SPICE-based modeling framework for the panel, using the compact model to describe individual subcells. The model is versatile and can be

This report is available at no cost from the National Renewable Energy Laboratory (NREL) at www.nrel.gov/publications.

used to study a broad range of phenomena. As an illustrative example, we study the reliability concern due to partial shading and associated redistribution of temperature close to and away from the shaded regions.

5 Acknowledgments

This work was supported by the U.S. Department of Energy under Contract No. DE-AC36-08GO28308 with the National Renewable Energy Laboratory, the U.S. Department of Energy under DOE Cooperative Agreement no. DE-EE0004946 ("PVMI Bay Area PV Consortium"), the National Science Foundation through the NCN-NEEDS program, contract 1227020-EEC, and by the Semiconductor Research Corporation. The authors would like to thank Piotr Szaniawski and Dr. Jian Li for experimental data and Prof. Marika Edoff, Prof. Jim Sites, Dr. Sarah Kurtz, and Prof. Mark Lundstrom for helpful discussion.

6 References

[1] A. Johansson, R. Gottschalg, and D. G. Infield, "Modelling shading on amorphous silicon single and double junction modules," in *Photovoltaic Energy Conversion, 2003. Proceedings of 3rd World Conference on*, 2003, pp. 1934–1937 Vol.2.

[2] S. Dongaonkar, C. Deline, and M. A. Alam, "Performance and reliability implications of two-dimensional shading in monolithic thin-film photovoltaic modules," *IEEE J. Photovoltaics*, vol. 3, no. 4, pp. 1367–1375, 2013.

[3] S. Dongaonkar and M. A. Alam, "End to end modeling for variability and reliability analysis of thin film photovoltaics," in *IEEE International Reliability Physics Symposium Proceedings*, 2012.

[4] D. A. R. Barkhouse, O. Gunawan, T. Gokmen, T. K. Todorov, and D. B. Mitzi, "Device characteristics of a 10.1% hydrazine-processed Cu2ZnSn(Se,S)4 solar cell," *Prog. Photovoltaics Res. Appl.*, vol. 20, no. 1, pp. 6–11, 2012.

[5] M. Gloeckler, C. R. Jenkins, and J. R. Sites, "Explanation of Light/Dark Superposition Failure in CIGS Solar Cells," *MRS Proc.*, vol. 763, p. B5.20, Jan. 2003.

[6] J. E. Moore, S. Dongaonkar, R. V. K. Chavali, M. A. Alam, and M. S. Lundstrom, "Correlation of Built-In Potential and I–V Crossover in Thin-Film Solar Cells," *IEEE J. Photovoltaics*, vol. 4, no. 4, pp. 1138–1148, Jul. 2014.

[7] J. L. G. R. V. K. Chavali, J. E. Moore, X. Wang, M. A. Alam, M. S. Lundstrom, "Frozen Potential Approach to Separate the Photo-Current and Diode Injection Current in Solar Cells," *IEEE J. Photovoltaics*, 2015.

[8] M. Hejri, H. Mokhtari, M. R. Azizian, M. Ghandhari, and L. Soder, "On the Parameter Extraction of a Five-Parameter Double-Diode Model of Photovoltaic Cells and Modules," *IEEE J. Photovoltaics*, vol. 4, no. 3, pp. 915–923, May 2014.

This report is available at no cost from the National Renewable Energy Laboratory (NREL) at www.nrel.gov/publications.

[9] M. T. Boyd, S. a. Klein, D. T. Reindl, and B. P. Dougherty, "Evaluation and Validation of Equivalent Circuit Photovoltaic Solar Cell Performance Models," *J. Sol. Energy Eng.*, vol. 133, no. 2, p. 021005, 2011.

[10] J. Merten, J. M. Asensi, C. Voz, a. V. Shah, R. Platz, and J. Andreu, "Improved equivalent circuit and analytical model for amorphous silicon solar cells and modules," *IEEE Trans. Electron Devices*, vol. 45, no. 2, pp. 423–429, 1998.

[11] S. S. Hegedus and W. N. Shafarman, "Thin-film solar cells: device measurements and analysis," *Prog. Photovoltaics Res. Appl.*, vol. 12, no. 23, pp. 155–176, Mar. 2004.

[12] X. X. Liu and J. R. Sites, "Solar-cell collection efficiency and its variation with voltage," *J. Appl. Phys.*, vol. 75, no. 1, p. 577, Jan. 1994.

[13] P. Szaniawski, J. Lindahl, T. Törndahl, U. Zimmermann, and M. Edoff, "Light-enhanced reverse breakdown in Cu(In,Ga)Se2 solar cells," *Thin Solid Films*, vol. 535, pp. 326–330, May 2013.

[14] S. Puttnins, S. Jander, a. Wehrmann, G. Benndorf, M. Stölzel, a. Müller, H. von Wenckstern, F. Daume, a. Rahm, and M. Grundmann, "Breakdown characteristics of flexible Cu(In,Ga)Se2 solar cells," *Sol. Energy Mater. Sol. Cells*, vol. 120, pp. 506–511, Jan. 2014.

[15] G. Tina, "A Coupled Electrical and Thermal Model for Photovoltaic Modules," *J. Sol. Energy Eng.*, vol. 132, no. 2, p. 024501, 2010.

[16] S. Armstrong and W. G. Hurley, "A thermal model for photovoltaic panels under varying atmospheric conditions," *Appl. Therm. Eng.*, vol. 30, no. 11–12, pp. 1488–1495, 2010.

[17] T. J. Silverman, M. G. Deceglie, X. Sun, R. L. Garris, M. A. Alam, C. Deline, and S. Kurtz, "Module-scale thermal and electrical effects of partial illumination in monolithic thin-film photovoltaics," *2015 IEEE 42nd Photovolt. Spec. Conf.*

[18] R. F. Pierret, *Semiconductor Device Fundamentals*. Prentice Hall, 1996.

[19] M. S. Lundstrom and R. J. Schuelke, "Numerical analysis of heterostructure semiconductor devices," *IEEE Trans. Electron Devices*, vol. 30, no. 9, pp. 1151–1159, 1983.

[20] T. Song, J. Tyler McGoffin, and J. R. Sites, "Interface-Barrier-Induced J–V Distortion of CIGS Cells With Sputtered-Deposited Zn(S,O) Window Layers," *IEEE J. Photovoltaics*, vol. 4, no. 3, pp. 942–947, May 2014.

[21] R. V. K. Chavali, J. R. Wilcox, B. Ray, J. L. Gray, and M. a Alam, "Non - Ideal Effects of Dark and Light I - V Characteristics in a - Si / c - Si Heterojunction," vol. 4, no. 3, pp. 763–771, 2014.

[22] U. Rau and H. W. Schock, "Electronic properties of Cu(In,Ga)Se 2 heterojunction solar cells-recent achievements, current understanding, and future challenges," *Appl. Phys. A Mater. Sci. Process.*, vol. 69, no. 2, pp. 131–147, Aug. 1999.

This report is available at no cost from the National Renewable Energy Laboratory (NREL) at www.nrel.gov/publications.

[23] C. Corwine, "Copper inclusion and migration from the back contact in CdTe solar cells," *Sol. Energy Mater. Sol. Cells*, vol. 82, no. 4, pp. 481–489, Mar. 2004.

[24] S. H. Demtsu and J. R. Sites, "Effect of back-contact barrier on thin-film CdTe solar cells," *Thin Solid Films*, vol. 510, no. 1–2, pp. 320–324, Jul. 2006.

[25] S. Ouédraogo, F. Zougmoré, and J. M. Ndjaka, "Numerical analysis of copper-indium-gallium-diselenide-based solar cells by SCAPS-1D," *Int. J. Photoenergy*, vol. 2013, 2013.

[26] M. Gloeckler, a. L. Fahrenbruch, and J. R. Sites, "Numerical modeling of CIGS and CdTe solar cells: setting the baseline," *3rd World Conf. onPhotovoltaic Energy Conversion, 2003. Proc.*, vol. 1, pp. 491–494, 2003.

[27] S. M. Sze and K. K. Ng, *Physics of Semiconductor Devices*, 3 Edition. Wiley-Interscience, 2006.

[28] H. Kufluoglu and M. A. Alam, "A computational model of NBTI and Hot Carrier Injection time-exponents for MOSFET reliability," *J. Comput. Electron.*, vol. 3, no. 3–4, pp. 165–169, 2004.

[29] H. Bentarzi, *Transport in Metal-Oxide-Semiconductor Structures*. Berlin, Heidelberg: Springer Berlin Heidelberg, 2011.

[30] S. Lany and A. Zunger, "Light- and bias-induced metastabilities in Cu(In,Ga)Se2 based solar cells caused by the (VSe-VCu) vacancy complex," *J. Appl. Phys.*, vol. 100, pp. 1–15, 2006.

[31] S. Silvestre, a. Boronat, and a. Chouder, "Study of bypass diodes configuration on PV modules," *Appl. Energy*, vol. 86, no. 9, pp. 1632–1640, 2009.

[32] D. Nguyen and B. Lehman, "A reconfigurable solar photovoltaic array under shadow conditions," *Conf. Proc. - IEEE Appl. Power Electron. Conf. Expo. - APEC*, pp. 980–986, 2008.

[33] S. Dongaonkar, J. D. Servaites, G. M. Ford, S. Loser, J. Moore, R. M. Gelfand, H. Mohseni, H. W. Hillhouse, R. Agrawal, M. a. Ratner, T. J. Marks, M. S. Lundstrom, and M. a. Alam, "Universality of non-Ohmic shunt leakage in thin-film solar cells," *J. Appl. Phys.*, vol. 108, no. 12, p. 124509, 2010.

This report is available at no cost from the National Renewable Energy Laboratory (NREL) at www.nrel.gov/publications.